Calculated Properties of Ag Clusters on Silver Halide Cubic Surface Sites

R. C. Baetzold

Imaging Research and Advanced Development, Eastman Kodak Company, Rochester, New York 14650-2021

Received: May 15, 1997[⊗]

The ionic and electronic steps in the initial photolysis of silver halide to form silver clusters have been analyzed by a combination of classical and quantum mechanical procedures. We have applied Hartree−Fock and local density methods to the problem and included treatment of the long-range lattice polarization. It is found that the electron-accepting and hole-accepting levels of these clusters depend strongly upon their site of adsorption. The positive kink is a favorable site for growth where electrons from the conduction band can be trapped prior to neutralization by interstitial silver ions. It is shown that relaxation of the cluster geometry following electron capture is an important means of deepening the electron trapping level. Hole trapping is possible at some of these clusters, leading to a reduction in their size. Overall, the picture that emerges is consistent with the generally accepted nucleation and growth mechanism of photolysis.

1. Introduction

The photolysis of silver halide is the basis for photographic technology. This process has been understood in terms of an overall picture based upon experimental results and shaped into phenomenological models. There are multiple ionic and electronic steps that occur following absorption of a photon by silver halide. The models that have been deduced are nevertheless rather sophisticated and have been successful in explaining and motivating the design of experiment. The most commonly cited mechanism[1] is termed the nucleation and growth model. It represents a skillful synthesis of experimental results and deductions, based upon physical measurements in silver halide, that has evolved over the years through the efforts of many workers. This mechanism has been cast in mathematical terms and explored in Monte Carlo type calculations[2] and in calculations of increasing complexity.[3] Other mechanisms that have received some attention include a thermodynamic treatment of silver cluster formation[4a−c] and a photoaggregation model.[4d] These latter mechanisms are beyond the scope of the present study.

The steps in the nucleation and growth model of latent image formation have been summarized by Hamilton.[1,2b] These steps rest upon many different experimental results, yet it is difficult to prove the entire microscopic mechanism in such a complicated system. The main steps are plotted in Figure 1. The photoelectrons are generated by absorption of photons, and the silver ions are mobile interstitial ions. There is an electrostatic driving force for this sequence of steps. The positive kink has a formal charge of $+^1/_2$ as derived through symmetry arguments or Madelung consideration at the surface positive kink and provides a shallow temporary electron trapping site. Shallow trapping of electrons at defects in silver halide has been well established.[5] This site is converted to a site with the formal charge $-^1/_2$ upon electron trapping. This charge is attractive for the interstitial silver ion, and upon attraction to this site the formal charge is converted back to $+^1/_2$. At this point an unstable silver atom has been created at the kink site. The sequence can be repeated with the next photoelectron being attracted to the Ag atom at the kink site where the charge is now $+^1/_2$. Movement of another silver ion to this site leads to the formation of Ag_2, which is a nucleation center because this species is stable. These steps can be repeated with the arrival

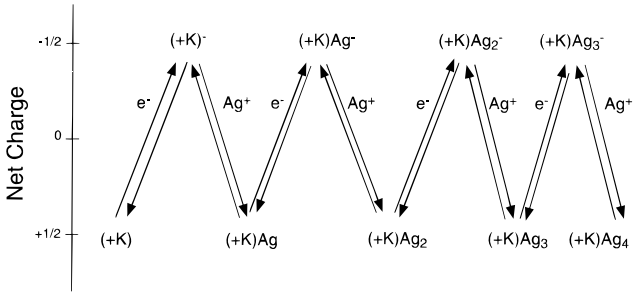

Figure 1. Sketch of the stepwise mechanism of electron and interstitial silver ion capture at a positive kink site leading to nucleation and growth of a silver cluster.

of additional photoelectrons and interstitial silver ions. The stage after Ag_2 formation is termed growth and eventually leads to a center large enough to catalyze photographic development. In development, electrons are transferred from a reducing agent in solution to the silver center, which causes a chemical reduction of silver halide to silver. It should be stressed that the initial steps in photolysis are reversible, leading to an unstable Ag atom state. We will investigate the energy changes involved in these reaction steps.

The photohole is not included in Figure 1, but it does play an important role in the nucleation and growth model. The photohole can react with an electron to annihilate each carrier. In the indirect bandgap materials AgCl and AgBr, there is a symmetry restriction on free hole plus free electron recombination, but if one of the carriers is in a trap state, there is no such restriction. There are shallow electron traps for the electron in the presence of positive surface kinks and interstitial silver ions and for the hole in the form of negative surface kink sites. The hole can also migrate to a silver cluster and oxidize it. These reactions compete with the efficient transformation of photoelectrons into silver clusters.

We,[6] and others,[7−9] have made attempts to computationally study the properties of silver clusters adsorbed to silver halide. Our work[6b,c] showed that the properties of the silver cluster were modified by the silver halide substrate and, in particular, the structure of the site where the cluster was adsorbed. Of course these calculations were rather simplified, employing a semiempirical CNDO method and treating only a few silver halide ions. The effects of lattice polarization could only be partially included in these calculations. Despite these limitations, several

[⊗] Abstract published in *Advance ACS Abstracts,* September 1, 1997.

S1089-5647(97)01625-8 CCC: $14.00

TABLE 1: Properties of Gas Phase Silver Clusters

size	geometry[a]	bond length (Å)	total bond energy (eV)	ionization potential (eV)	electron affinity (eV)[b]
1				7.57	1.30
2		2.530[c]	1.64[c]	7.56[d]	1.06
3	obtuse triangle		2.63[e]	6.20[f]	2.43
4	rhombus			6.65[g]	1.65
5	planar			6.35[g]	2.11
6	pentagonal pyramid			7.15[g]	2.06

[a] Reference15 calculation. [b] Ho, J.; Ervin, K. M.; Lineberger, W. C. *J. Chem. Phys*. **1990**, *93*, 6967. [c] Ran, Q.; Schmude, R. W.; Gingerich, K. A.; Wilhite, D. W.; Kingcade, *J. Phys. Chem*. **1993**, *97*, 8535. [d] Morse, M. D. *Chem. Rev*. **1986**, *86*, 1049. [e] Hilpert, K.; Gingerich, K. A. *Ber. Bunsen-Ges. Phys. Chem.* **1980**, *84*, 739. [f] Alameddin, G.; Hunter, J.; Cameron, D.; Kappes, M. M. *Chem. Phys Lett*. **1992**, *192*, 122. [g] Jackscharth, C.; Ragin, I.; Schulze, W. *Z. Phys. D* **1992**, *22*, 517.

trends were found including an odd−even oscillation in the ionization potential (IP) in which even-sized clusters were more difficult to oxidize than the adjacent odd-sized cluster. Also the IP of Ag_2 was greater than the valence band edge for clusters adsorbed to sites of partial positive charge. This is in contrast to results calculated at sites of neutral or partial negative charge where the IP of Ag_2 is less than the valence band edge. Thus, only the latter could be oxidized by a photohole. The odd−even oscillation for adsorbed clusters was confirmed in the interpretations of the measurements of photoionization thresholds by Kawasaki et al.[10] Measurements of gas-phase Ag_n clusters[11,12] have also shown the same type of odd−even oscillation in IP and electron affinity (EA). Interpretations[13] of photographic experiments have supported the nonreactivity of holes with Ag_2, as long as the cluster is located at a site of positive charge.

In the meantime, there have been several advances in computational methodology. For example, there have been a variety of high-quality quantum mechanical calculations on gas-phase silver clusters.[14−17] Local density and Hartree−Fock methods with electron correlation treatments have been employed, and now with efficient computer programs, improved computers can be applied to realistic models of the photographic system. In the gas phase it was found that neutral small clusters tend to be planar. For example, recent calculations give Ag_3 as triangular,[15] Ag_4 as rhombic,[16] Ag_5 as trapezoidal,[16] and Ag_6 as trigonal.[16] The calculated ionization potential and electron affinity oscillate between odd- and even-sized clusters. The best calculations using electron correlation methods, but not explicit relativistic effects, get ionization potentials accurate within a few tenths of an electronvolt for silver clusters. A collection of experimental data for the small clusters is given in Table 1. These data are useful for testing calculations and understanding the general properties of silver clusters. At the same time, methods for treating lattice polarization have advanced considerably. Treatment of this effect in silver halide is essential because of its long-range nature, which can stabilize defects by as much as several electronvolts. The HADES methodology[18] incorporating the Mott−Littleton approximation[19] has proven to be reliable for bulk ionic solids. This method has been extended to surfaces,[20] and so there is now a means to advance the computational treatment of silver clusters adsorbed to silver halide.

In performing calculations relevant to silver halide photolysis, we must define the working surface. We consider only cubic (100) surfaces in this work. Typically, such a surface in an emulsion grain contains various organic and inorganic molecules. We will be concerned with the bare or uncovered portions of such a surface and consider that such regions can exchange ionic species including Ag^+ with surrounding covered surface regions.

This paper represents an attempt to computationally study the energetics of steps involved in the growth of silver clusters during photolysis of silver halide. We focus on steps important in the nucleation and growth mechanism.[1] In section 2 we describe two methods of calculation. One is a classical simulation of surfaces using the Mott−Littleton approximation and the other is a quantum mechanical method, which relies on the classical calculation for polarization corrections. In section 3 we describe the results for ionic steps involving silver ion and electronic steps involving electrons or holes. Finally, in section 4, we discuss these results and compare to the nucleation and growth model and various experimental results.

2. Method

Classical Atomistic Calculations. Classical atomistic calculations have been applied to a variety of ionic crystal surfaces[20,21] including silver halide.[22] These calculations can be used to treat periodic two-dimensional planes of ions, or a single defect, on a surface interacting with the rest of the crystal. The computer codes MIDAS and CHAOS[20] perform these tasks, respectively. The Mott−Littleton procedure[18] is used to treat the ions around a defect. All ions in a hemispherical region surrounding the defect are allowed to relax to achieve zero force on each ion within the framework of the interatomic potential. Longer range effects beyond 6−7 interatomic distances are treated by continuum methods. More complete discussions of this methodology are available.[18,21]

Accurate interatomic potentials are key to utilizing classical atomistic methods. Coulomb terms are treated within the scope of the shell model.[23] Formal unit net charges are assigned to ions and all of the long-range interactions are treated, although this does not imply a fully ionic crystal.[23b] The short-range interactions representing the overlap of electron clouds are expressed in the Buckingham form

$$V(r) = A \exp(-r/\rho) - C/r^6 \qquad (1)$$

where r is the distance and A, ρ, and C are fitted constants. Several years of development of potentials for silver halide[24−26] have yielded excellent representations for the bulk crystal. These accurately describe dielectric, elastic, and cohesive properties of the perfect crystal, as well as Frenkel defect formation energies and their temperature dependence. They do have some shortcomings in terms of describing defect migration energies. More complete discussions[25] of these potentials are available. We employ the potentials from ref 26 involving explicit two-body short-range terms.

We need to construct models containing various surface defect structures since earlier work[6] has shown that the properties of silver clusters depend upon the site where they are adsorbed. Figure 2 contains the single and double kink sites on cubic surfaces, which appear to be important. In the positive kink model (+K) an additional atom may be adsorbed right next to three positive ions. This adsorption site and the nearby region of space behaves as if the site possesses a partial positive charge,

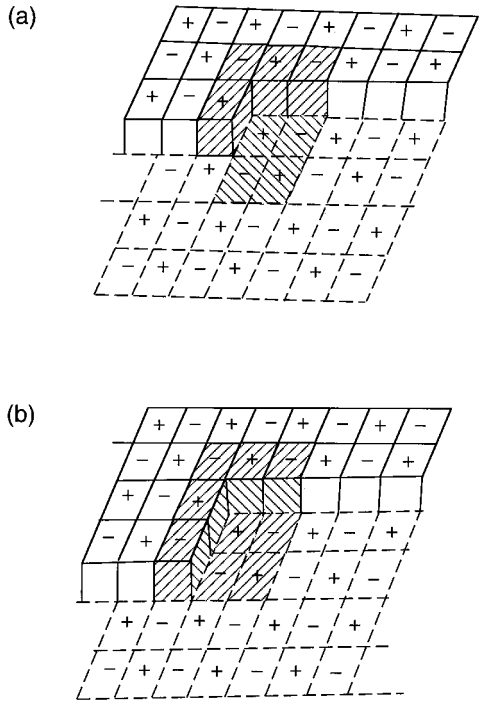

Figure 2. Surface models showing the arrangement of ions at a single positive kink (+K) in (a) and a double kink (+DK) in (b). The corresponding negative single (−K) kink or negative double kink (−DK) is generated by interchanging positive and negative ions. Shaded ions represent ions treated by quantum mechanical methods and embedded in point charges.

in accordance with the considerations originally developed by Seitz.[27] The same considerations lead to a partial negative charge at the site obtained by interchanging all of the positive ions with negative ions. This type of model is termed a negative kink (−K) and is not shown because of its obvious similarity to the positive kink. The double kink model is shown in Figure 2b. Here, a second ledge extends right up to the kink so that there is a pair of positive ions balanced by a pair of negative ions right in the vicinity of the kink site. Thus this site is thought to be neutral in charge relative to the single kink sites. There are two possible types of double kinks depending upon the placement of positive (+DK) or negative ion pairs (−DK) on the inner corner of this site. There is also the ledge (step) of monatomic height, which is part of the kink models shown in Figure 2 and which may act as an adsorption site. The flat cubic surface (100) is also a potential adsorption site. The adsorption sites considered may be constructed within the scope of the atomistic procedures. In fact, we have previously shown[28] how to construct these models and used them to study silver ion interstitial and vacancy generation at silver halide surfaces. The flat (100) and stepped (501) silver halide surfaces were used to generate these surface defects. A partial row of 12 ions along the step ledge with respect to the infinite surface representation is removed to create a positive or negative kink site. The double kink is generated by removing two rows of 12 ions each along the ledge.

Interatomic potentials required for the interaction of cluster silver atoms with the surface ions were computed using a local density method with the BLYP functional.[29] In the case of a kink site on AgCl, we constructed a $(Ag^+)_3(Cl^-)$ unit attached on an array of point ions that represented a positive kink. The Ag atom is moved along a trajectory equidistant from the three Ag^+ ions and the resulting interaction energy fitted to eq 1 to give an interaction term for each Ag^+-Ag^0. Corresponding terms for Cl^--Ag^0. are determined using a $(Cl^-)_3(Ag^+)$ negative kink unit. For (100) surfaces we compute interactions between Ag^0 and $(Ag^+)_2(Cl^-)_2$ units in a flat surface. Corresponding potentials are determined for AgBr surface sites. The calculations employed a model potential[30] on Ag and double ζ plus polarization basis sets[31] throughout. The interatomic potentials that were determined are given in the Table 11 of the Appendix.

Interatomic potentials for the interaction of cluster atoms with one another were determined using Hartree−Fock plus Moller−Plesset second-order perturbation theory (MP2). The gas-phase cluster underwent a uniform breathing motion deformation in order to vary the internuclear distance. The total interaction energy corrected for the number of interactions was fitted to eq 1, and parameters are given in the Appendix. We treated relevant charge states of the cluster and considered linear triatomic and square tetratomic structures to determine these parameters.

Quantum Mechanical Calculations. A treatment of silver clusters adsorbed to silver halide surfaces requires some approximations. An array of cluster atoms and a few silver halide ions are attached to a point-ion array. The cluster and silver halide ions are treated quantum mechanically in the Madelung field created by the point-ion array. Short-range interatomic terms are used to describe the interaction of the quantum mechanical ions with adjacent point ions. The total energy including components due to the Coulomb potential and short-range terms is computed and an optimized structure for the cluster atoms is determined. At the conclusion of this calculation a second calculation is applied in order to estimate the lattice polarization energy. We fix the cluster ions in position and determine the change in energy due to polarization of the silver halide ions. A classical atomistic calculation, as described above, is employed. We start with ion positions and corresponding Mulliken charges determined from the quantum mechanical part of the calculation and allow the remaining silver and halide ions represented by the shell model to relax to final equilibrium positions in order to compute the corresponding change in energy. This energy change is added to the total quantum mechanical energy with subtraction of the short-range terms in the quantum mechanical calculation in order to avoid double counting. This procedure gives the total energy and is a practical means of including this lattice polarization.

The models used in this work consist of approximately ten silver and halide ions attached to the point ions. The kink site is modeled with a quantum mechanical unit Ag_4Cl_4, which is indicated by the shaded ions in Figure 2a. The double kink was treated with a Ag_4Cl_5 unit as indicated in the shaded part of Figure 2b. The (100) flat surface was treated with a Ag_5Cl_4 single layer array having C_4 symmetry. Approximately 1200 point ions are attached to these quantum mechanical units. The array has roughly a hemispherical shape with the quantum mechanical unit mounted on the flat side. The point charges are located at silver and halide positions appropriate to the perfect crystal. The overall unit is prepared to have zero charge prior to adsorption of the silver clusters. The atoms or ions in the silver cluster are treated with a model potential[30] representing the core electrons. The 4p, 4d, and 5s valence electrons are outside the pseudopotential and can be treated by two radial functions per orbital (double ζ, DZ) or double ζ plus polarization (DZP) basis sets given in earlier work.[31] Corresponding basis functions were chosen for the Au atom. The bromine and chlorine atoms were treated with a double ζ plus polarization full basis set. The Hartree−Fock procedure with or without Moller−Plesset second-order perturbation theory (MP2) or local density methods at the BLYP level[29] are employed within the

TABLE 2: Adsorption Energy (eV) of Ag Clusters on AgCl Surface Sites Calculated by the Classical Atomistic Method

cluster	+K	−K	+DK	−DK	flat
Ag	2.28	2.60	2.36	2.17	0.55
Ag^+	3.70	4.74	3.15	4.15	3.48
Ag_2	4.52	4.66	5.00	5.06	1.10
Ag_2^+	5.51	7.11	6.67	6.89	2.34
Ag_3	7.28	7.92	7.72	7.90	2.65
Ag_3^+	7.69	9.67	7.90	9.18	3.64
Ag_4	8.48	8.40	9.75	9.93	2.62
Ag_4^+	9.27	9.35	10.78	11.32	3.50

TABLE 3: Adsorption Energy (eV) of Ag Clusters on AgBr Surface Sites Calculated by the Classical Atomistic Method

cluster	+K	−K	+DK	−DK	flat
Ag	2.01	2.23	1.89	2.21	0.92
Ag^+	3.10	4.45	2.62	3.77	3.34
Ag_2	3.89	5.47	3.47	3.17	1.49
Ag_2^+	4.54	6.03	5.01	5.29	3.51
Ag_3	6.34	6.35	6.22	6.09	2.02
Ag_3^+	6.98	8.21	6.93	7.58	3.61
Ag_4	7.39	6.89	6.93	7.42	4.12
Ag_4^+	7.90	8.74	7.10	7.78	5.30

CADPAC computer code.[32] Open-shell cases are treated by the restricted open-shell procedure (ROHF).

The ionization potential and electron affinity are calculated by total energy difference of the appropriate charge states. These resulting values are corrected for deficiencies in the calculation due to incomplete basis sets and correlation energy terms. We estimate this term from the calculated value of the gas-phase Ag cluster compared to the experimental data in Table 1. These correction terms are given for the Hartree−Fock calculations with a DZ basis and BLYP calculations using a DZ plus polarization basis in Table 12 of the Appendix. As expected, the correction terms are much smaller for the BLYP calculation. In the same table, we give the calculated lattice polarization terms at different crystal sites. All of these terms are applied in additive form to the calculated values. This represents the best practical way of treating lattice polarization within the scope of a cluster model. An improvement would involve a more self-consistent procedure.

3. Results

Classical Atomistic Calculations. *Silver Cluster Structure and Energy.* The adsorption energy of neutral and charged silver clusters attached to silver halide is computed in order to determine various physical properties. This quantity is determined by placing an array of silver atoms near a surface site such as those in Figure 2 and allowing all atoms and surface ions to relax to their equilibrium positions. The adsorption energy is the change in total energy from the separated relaxed cluster and surface to the relaxed surface containing the adsorbed cluster. Adsorption energies for various clusters at 0 K on different silver halide surface sites are reported in Tables 2 and 3. The adsorption energies, which are calculated for silver clusters to silver halide, are significant and represent bonding effects. These values will be used to compute the energy changes of various surface processes. The equilibrium structure corresponding to clusters is found to be near planar, just as is found in gas-phase calculations.[14] Figure 3 is a sketch of the calculated structure of neutral clusters near positive and double kinks on silver bromide. The clusters do not occupy the virtual lattice sites where the next lattice ions would be expected to occupy. Rather, they occupy low symmetry sites with some distortions normal to the surface. It is interesting that the dimer occupies a site with its bond midpoint closest to the kink sites,

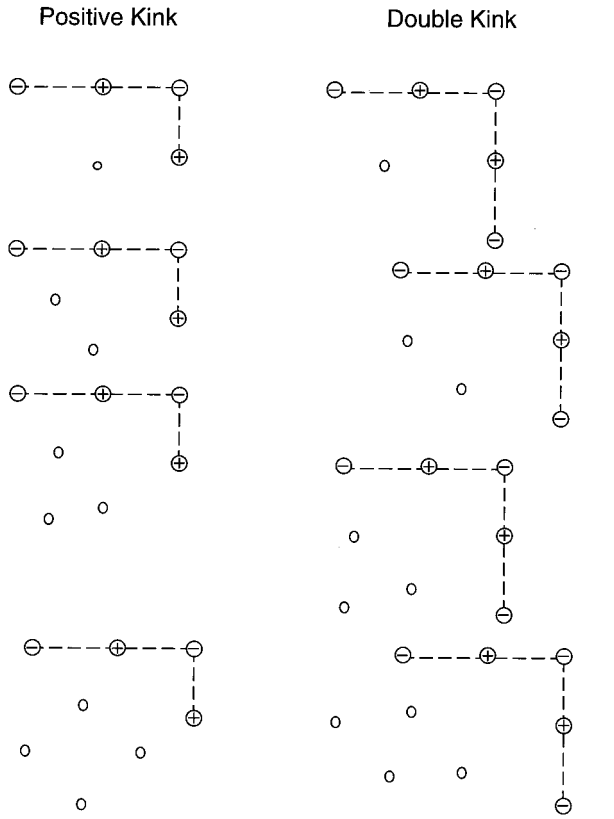

Figure 3. Sketch of the top view of the computed structure of neutral silver clusters near positive kinks (+K) or double kinks (+DK) on AgBr surfaces. The lattice ions along the upper edge of the kink site are denoted by + or −, and the silver atoms, by ○ in the figure.

and this pattern continues on to the larger clusters. At the flat surface, the cluster atoms tend to occupy sites near the hollow on (100) surfaces and take on triangular and square shapes. The shape of clusters adsorbed near the negative kink is similar to the shape of those adsorbed near the positive kink. We note that the cluster shapes are similar on AgCl surfaces.

Stability of the Silver Atom State. The stability of the silver atom state is calculated by evaluating the energetics of the reversible reaction

$$Ag^0 \leftrightarrow Ag^+ + e_{cb} \tag{2}$$

where we consider the atom is adsorbed at some surface defect site, the electron goes to the bottom of the conduction band (e_{cb}), and the Ag^+ is adsorbed on the surface at a negative kink, which we assume to be present in excess due to the negative surface potential of silver halide. We have taken this surface negative kink site as a reference state because it represents the surface site of strongest binding for a silver ion. To use the calculated energies in Tables 2 and 3, a value must be obtained for the crystal electron affinity that is the energy at the conduction band edge. This value is taken as 4.51 eV in AgCl and 4.57 eV in AgBr. These values were calculated[33] at 300 K from the photoemission threshold[34] for epitaxial films prepared in vacuum and the measured optical indirect bandgap.[35] Thus the energy of reaction 2 may be calculated from a thermodynamic cycle in which the atom is desorbed from the surface to the gas phase, ionized, and readsorbed with the electron going to the bottom of the conduction band. The energy change for reaction 2 is

$$\Delta E = E_1(0) - E_1(+) - \lambda + \mathrm{IP}_1 \tag{3}$$

TABLE 4: Calculated Energy (eV) of Ag Atom Decay on Silver Halide Surface Sites

site	AgCl	AgBr
+K	0.63	0.62
−K	0.95	0.84
+DK	0.71	0.50
−DK	0.52	0.82
flat	−1.10	−0.43

TABLE 5: Trend in Ionization Energies (eV) for Ag_n Clusters on Different Sites Calculated by Atomistic Method

	AgCl cluster size			AgBr cluster size		
site	2	3	4	2	3	4
+K	2.07	1.28	1.35	2.35	0.99	1.57
−K	0.61	−0.06	1.19	2.44	−0.23	0.23
+DK	1.39	1.51	1.11	1.46	0.92	1.91
−DK	1.23	0.41	0.75	0.88	0.14	1.72
flat	1.82	0.70	1.26	0.98	0.04	0.90

where $E_1(c)$ is the adsorption energy of the single atom with charge c, λ is the crystal electron affinity or conduction band edge, and IP_1 is the gas-phase ionization potential of the silver atom (7.56 eV). We present the results of this calculation in Table 4. We observe stability of the silver atom of a few tenths of an electronvolt with respect to decay by reaction 2 except at the flat (100) surface. These values are in line with estimates of the Ag atom trap depth deduced from photographic measurements[36] that are in the range of 0.5 eV. Thus, a thermally activated decay of the silver atom can occur according to Boltzmann statistics and the calculations are consistent with reaction 2 being reversible.

Stability of Ag_n, $n \geq 2$. We may estimate the trends in stability of silver clusters on silver halide with respect to loss of an electron to the conduction band. We construct a thermodynamic cycle to compute the energy of the reaction

$$Ag_n^{\,0} \rightarrow Ag_n^{\,+} + e_{cb} \tag{4}$$

in the same way that we considered the stability of the single atom state. We compute the energy of reaction 4 as

$$\Delta E = E_n(0) - E_n(+) - \lambda + IP_n \tag{5}$$

where IP_n is the experimental gas-phase ionization energy (Table 1) for the cluster of size n atoms. We compute the values in Table 5 from the calculated adsorption energies in Tables 2 and 3.

Silver clusters with $n \geq 2$ are stable at the positive kink site. The energy required to ionize the cluster is greater than 1 eV and so the neutral clusters should have a long lifetime at these sites on AgCl and AgBr. The double kinks with positive inner ions are also reasonably stable sites for these Ag_n clusters. Generally, the silver clusters are less stable at the other sites. The important distinction between single atom and multiple atom clusters with respect to loss of an electron to the conduction band is the possibility that the multiple atom cluster does not have to release a silver ion simultaneously with electron release. It should be noted that only the trends for the data shown in Table 5 are considered significant. Absolute values of the energy levels require quantum mechanical calculations that are given later in this report.

Addition of Ag^+ Ions to Ag Clusters. We can employ atomistic calculations to examine the energy change for Ag^+ addition or removal from Ag clusters. The surface reaction

$$Ag_n^{\,0} + Ag^+ \rightarrow Ag_{n+1}^{\,+} \tag{6}$$

TABLE 6: Calculated Energy Change[a] (eV) for Addition of Ag^+ to Neutral Cluster

n	site	AgCl ΔE (eV)	AgBr ΔE (eV)
1	+K	−0.01	0.40
	−K	−1.29	−0.87
	+DK	−1.09	−0.19
	−DK	−1.50	−0.15
	flat	1.43	0.34
2	+K	0.21	0.00
	−K	−1.63	0.35
	+DK	0.48	−0.37
	−DK	−0.74	−1.32
	flat	0.82	0.97
3	+K	0.34	0.48
	−K	−0.10	−0.35
	+DK	−0.73	1.26
	−DK	−1.09	0.35
	flat	1.48	−1.24

[a] Negative energy indicates exothermic reaction.

has an energy change

$$\Delta E = E_n(0) - E_{n+1}(+) + E_1(+) - BE_n \tag{7}$$

where we take $E_1(+)$ as the reference binding energy of a silver ion to a negative surface kink and BE_n is the calculated binding energy of a silver ion to the neutral cluster of size n.

The results in Table 6 show a strong dependence of Ag^+ adsorption energy on the site of the silver halide surface. On the positive kink site and flat (100) surfaces, addition of a silver ion to the neutral silver cluster is generally endothermic and an unlikely reaction. At negative kinks the energy of reaction favors addition of Ag^+ to the cluster. Thus, at the negative kink the $Ag_{n+1}^{\,+}$ cluster is generally favored. This may be viewed as equivalent to a neutral cluster at the positive kink. At double kinks the formation of $Ag_{n+1}^{\,+}$ is more strongly favored if the inner ions are anions. Overall, these values are consistent with the surface sites having partial charges, as in the considerations inherent in Figure 1.

Stability of Ag_2^+. The Ag_2^+ species has an experimental[37] bond energy of 1.72 eV in the gas phase, which accounts for its stability. Consider the reaction

$$Ag_2^{\,+} \rightarrow Ag^0 + Ag^+ \tag{8}$$

at different sites in the crystal on the AgCl on AgBr surface. This reaction will proceed at flat surfaces and at the positive kink site according to the calculated data in Table 6. At other surface defect sites the reaction is unfavorable. The only way that reaction 8 could be made exothermic at these other sites is by the addition of agents to the surface that bind Ag^+ more strongly than the negative kink sites. Organic molecules may bind Ag^+ ions and might be a route through which Ag_2^+ could be made to decompose.

Quantum Mechanical Calculations. *General Features.* We examined various levels of calculation for the Ag_2 molecule to give an indication of the errors that can be expected in these calculations. The variables explored include the Hartree−Fock or local density method (BLYP),[29] whether the Ag model potential[30] has 17 (MPP) or 11 (MP) valence electrons, and the type of valence basis set on Ag. Table 7 compares results from various levels of calculation for Ag_2 with experiment. As expected on general considerations, good agreement with experiment on the various physical properties must include treatment of electron correlation and a basis set with polarization functions. The calculations treating adsorbed Ag clusters were performed at DZ or better basis sets using Hartree−Fock or the local density method.

TABLE 7: Calculated Properties of Ag_2 Gas Phase Clusters

method[a]	pseudopotential	basis[c]	*R* (au)	BE (eV)	IP (eV)	EA (eV)
HF	MPP	DZ	5.226	0.15	5.84	−0.09
HF	MPP	DZ + pol	5.196	0.36	5.58	−0.02
HF/MP2	MPP	DZ	5.148	0.63	6.44	−0.07
HF/MP2	MP	DZ + pol	4.898	1.50	6.85	0.47
HF/MP2	MPP	DZ + pol	4.878	1.60	7.11	0.58
BLYP	MPP	DZ	5.122	1.53	8.05	0.84
BLYP	MPP	DZ + pol	5.025	1.59	7.94	0.93
Exp.			4.781	1.64	7.57	1.06

[a] Symbols: Hartree−Fock, HF; Moller−Plesset second-order theory, MP2; local density BLYP. [b] The pseudopotential has 17 (MPP) or 11 (MP) valence electrons. [c] The valence basis set of silver is double ζ (DZ) and contains polarization functions of the p, d, or f type. [d] The calculated properties include equilibrium bond length (*R*), total bond energy (BE), ionization potential (IP), and electron affinity (EA).

Electron Trapping at a Positive Kink. The electron trapping at a structural defect site on the surface of silver halide is a reversible process because of the shallow trap depth. Electrons present in the conduction band of silver halide are free, but subject to Coulombic trapping by sites such as the positive kink site with a formal +1/2 charge. Based upon microwave photoconductivity experiments, proposals were advanced[38] that the electron is initially trapped into this shallow Coulomb trap at the kink followed by a structural relaxation of the lattice leading to a deeper trap state. A configuration coordinate diagram was drawn[38] with an activation barrier for conversion from the Coulombic state to the deeper relaxed state, as caused by strong coupling of the electron to the silver halide lattice.

We have investigated the possibility of forming the relaxed trapping state of the electron. Two different positive kink models were studied. The first is the Ag_4Cl_4 model of Figure 2 where the eight quantum mechanical ions are attached to the rigid point-ion array described before. This model is treated by the BLYP functional using double ζ plus polarization basis sets. The positive kink is first relaxed to zero strain. Then an extra electron is added and further relaxation is permitted. We find that such additional relaxation occurs with an energy lowering of 0.17 eV. We also tested this possibility using the slightly larger Ag_6Cl_6 quantum mechanical unit attached to the point ion array. Using double ζ basis sets and the SCF/UHF calculations, we find an energy lowering of 0.45 eV upon permitting relaxation of the electron trapped state at the positive kink. The results of both of our model calculations support the proposal discussed by Hamilton[39] that there is a strong coupling of the electron with the silver halide lattice at structural defect sites. Thus, surface positive kinks can become trapping states for an electron with a trap depth of a few tenths of an electronvolt. This trap depth is considerably larger than the few hundredths of an electronvolt thought possible just through a Coulombic trap.

Adsorbed Ag_n Cluster Models. The trapping of electrons or holes at a silver cluster will be determined by the cross sections and the potential trap depths for these processes. The cross section is largely determined by the net charge of the center, although other factors can be important.[39,40] We will consider trap depths for various events. These are calculated from the total energy differences of initial and final states and represent thermal trap depths since lattice relaxation is included in the calculation. We have referenced our results to a calculation for an octahedral $AgCl_6^{5-}$ unit embedded in a sphere of point ions and treated with the same basis sets and method of polarization corrections applied to the adsorbed silver clusters. We compute 6.75 and 3.55 eV for the AgCl valence band and conduction band edges, respectively. We have placed the AgBr band edges at 3.55 and 6.15 eV by lining up the AgCl and AgBr conduction band edges.

We first treated silver clusters on AgCl at a variety of surface defect sites using Hartree−Fock methods. A small cluster of AgCl ions was embedded into an array of point ions with zero overall charge in order to represent the substrate for silver cluster adsorption. The array had a roughly hemispherical shape. We employ clusters of Ag_4Cl_4 for positive and negative kinks, Ag_4Cl_5 for the double kink, and Ag_5Cl_4 for the flat surface. These clusters and point-ion arrays have been described earlier. We place a Ag_n cluster on these defect sites and perform a geometry optimization for $n = 1-4$. The shapes found for the optimized geometry are roughly planar and very similar to the shapes found in the atomistic calculation.

TABLE 8: Hartree−Fock Calculated IP and EA Values (eV) for Ag Clusters Adsorbed to Different AgCl Surface Site Models

site	cluster model	cluster size	IP	EA
+K	Ag_4Cl_4	1	5.96	4.55
		2	7.15	3.74
		3	5.18	4.17
		4	7.13	4.68
−DK	Ag_4Cl_5	1	6.61	2.77
		2	5.87	2.36
		3	3.93	3.00
		4	4.86	3.42
−K	Ag_4Cl_4	1	4.77	1.52
		2	3.77	0.96
		3	2.49	2.73
		4	3.27	3.03
flat	Ag_5Cl_4	1	5.77	2.94
		2	4.34	2.16
		3	2.47	3.07
		4	4.26	2.44

The ionization potentials and electron affinity are computed from the total energy differences at these optimized geometries. As indicated earlier, we correct the calculated IP and EA values for lattice polarization and deficiencies in the calculation due to basis set limitations or correlation energy corrections. We show these values for a SCF/ROHF calculation with the data in Table 8. The ionization potentials and electron affinities are plotted in Figure 4 for silver clusters adsorbed to AgCl. The trends with cluster size and adsorption site are significant. We call attention to the oscillations in IP and EA from 2 to 3 to 4 atom clusters generally found, the larger values are characteristic of the positive kink site, and observe that the IP of Ag_2 is greater than the valence band edge only at the positive kink site. The Ag_2 cluster and Ag_4 cluster at the positive kink will not be oxidized by a hole. On all of the other sites the ionization potential is small enough so that the hole can be trapped at all cluster sizes. The electron affinity of all Ag_n clusters at the positive kink is large enough to capture electrons from the bottom of the conduction band. At the other sites, the electron affinity values are much smaller and insufficient to capture photoelectrons from the conduction band.

We may examine the different-sized cluster properties shown from the data in Figure 4. The Ag atom has a large IP that is consistent with facile formation of a silver atom, and its decay

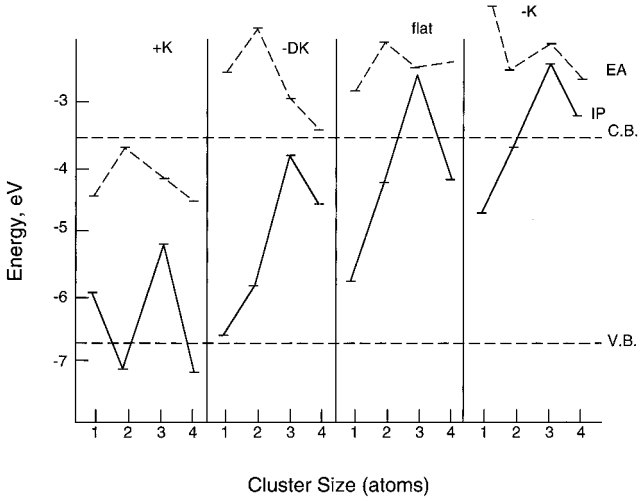

Figure 4. Calculated IP and EA for different sized silver clusters adsorbed to AgCl surface sites. This calculation is performed at the Hartree−Fock level using a double ζ basis set and corrections for polarization, correlation ,and calculation deficiencies as described in the text.

must first occur by loss of a silver ion, as in reaction 2. The EA of Ag is about 1.0 eV below the conduction band edge at the positive kink, making it a suitable site for electron capture. The calculated Ag_2 EA lies just under the conduction band edge, making it a temporary trap for photoelectrons. The Ag_3 cluster is particularly interesting because its IP and EA are very close in value at all of the sites. This species can trap electrons or holes at the positive kink because the IP and EA lie in the bandgap, causing this cluster to be rather unstable. The Ag_3 species will not be able to grow at the other sites by electron capture, because its EA value is sufficient to capture electrons only at the positive kink. The Ag_3 cluster has a IP value sufficient to capture holes at sites other than the positive kink. The Ag_4 cluster can capture photoelectrons when adsorbed at the positive kink.

These calculations allow for exchange of charge between the silver cluster and silver halide model unlike the classical atomistic calculations discussed before. The charges calculated by the Mulliken analysis are given in Table 13 of the Appendix. Inspection of these values suggests that very little charge is exchanged from the neutral or positively charged cluster with the silver halide. The anion state seems to allow a small part of its extra electron to be shared with the silver halide.

We now examine the energetics of silver clusters on AgCl surface sites in more detail using the BLYP functional. This should provide a more accurate calculation because some treatment of electron correlation is included in this method. The geometry of each cluster at the different adsorption sites was determined by a geometry optimization procedure in CADPAC.[32] The optimized structures tend to be planar, and relaxed coordinates are given for some of the clusters near the positive kink and double kink in Table 9. These computed structures are similar to the structures determined in the atomistic classical and Hartree−Fock calculations. A triangular and rectangular type of shape are found for Ag_3 and Ag_4, respectively. It can also be observed that the equilibrium positions change with the charge of the cluster.

We have computed the ionization potentials and electron affinities of these adsorbed clusters using the procedures discussed above. The calculated values are shown in Table 10 for the BLYP calculations on different sites of the cubic AgCl surface. We also consider some mixed AuAg clusters and plot all of these values in Figure 5 for analysis of the trends. The

TABLE 9: Computed Positions of Adsorbed Clusters to the Positive Kink Site Relative to the Site (000) in Au Units Using the BLYP Method

cluster	positive kink position (x, y, z)[a]		
Ag	0.172	0.639	0.061
Ag^+	0.608	0.378	−0.232
Ag^-	−0.083	0.569	0.199
Ag_2	−0.261	1.641	0.593
	4.590	−0.216	−0.025
Ag_2^+	0.262	1.601	−0.114
	6.488	−0.575	−0.557
Ag_2^-	0.054	1.106	0.514
	5.436	0.725	0.510
Ag_3	−0.245	1.294	0.866
	5.281	0.390	−0.035
	6.562	5.615	−0.209
Ag_4	−0.400	2.078	2.019
	3.511	0.215	−0.553
	6.068	5.415	−0.114
	3.174	9.964	0.054
cluster	double kink		
Ag	1.373	1.398	2.599
Ag^-	3.068	3.047	2.150
Ag_2	2.886	−0.752	1.476
	−0.696	2.895	1.577
Ag_2^+	2.954	−0.445	0.748
	−0.767	2.916	0.674
Ag_2^-	2.878	−0.744	1.461
	−0.880	2.958	1.727
Ag_3	3.490	−0.367	1.939
	0.065	3.576	2.229
	9.006	7.673	1.999
Ag_4	3.865	0.411	0.575
	−0.511	1.922	3.534
	4.797	4.797	2.001
	9.047	1.047	1.892

[a] The virtual site for addition of the next ion to the kink (000). The positive directions for x, y, z are away from this crystal site toward the vacuum.

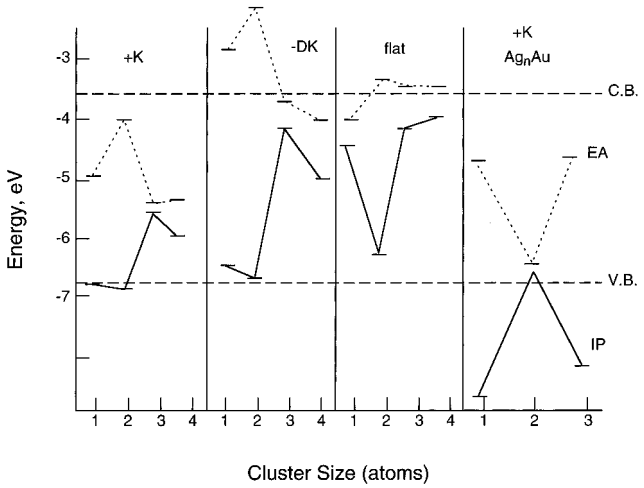

Figure 5. Calculated IP and EA for different sized Ag, Au, and AgAu clusters adsorbed to different AgCl surface sites using the BLYP functional calculation.

calculated trends with cluster size and adsorption site agree well with the Hartree−Fock calculations. All neutral clusters can accept conduction band electrons at the positive kink because their electron affinity is greater than the crystal electron affinity. The same is not true at the double kink or flat site. Thus, growth by the nucleation and growth model mechanism can proceed at the positive kink site, but not the other sites. Comparison of the data in Tables 8 and 10 does reveal differences in the calculated values for IP and EA using the two methods. There

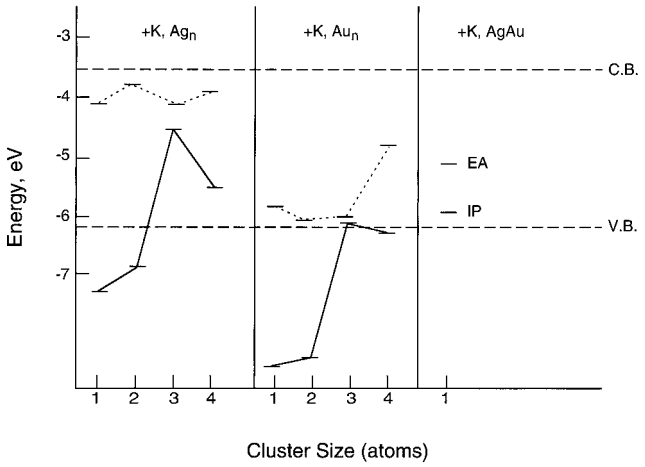

Figure 6. Calculated IP and EA for different sized Ag, Au and AgAu clusters adsorbed to the AgBr positive kink model (+K) using the BLYP functional calculation.

TABLE 10: Ionization Potential and Electron Affinity Values (eV) Calculated for Ag Clusters on AgCl Using BLYP Functional

cluster	site	IP	EA
Ag	+K	6.75	4.91
Ag_2		6.78	3.70
Ag_3		5.51	5.45
Ag_4		5.91	5.40
Ag	−DK	6.46	3.56
Ag_2		7.10	2.31
Ag_3		4.25	3.89
Ag_4		5.05	4.03
Ag	flat	4.47	4.13
Ag_2		6.37	3.61
Ag_3		4.20	3.70
Ag_4		4.08	3.70
Au_2	+K	9.80	3.96
AgAu		10.40	3.63
Ag_2Au		5.76	5.45
Ag_3Au		6.24	5.26

are slight differences in the calculated optimized geometries. The trends for data calculated by the two different methods well agree with one another. These trends include the oscillations in IP and EA between the 2−3−4 atom clusters, the shifts due to site of adsorption, and the unique electron capture ability at the positive kink. Again we find unique properties for Ag_2 on the positive kink. It cannot capture photoholes but is a temporary electron trap. In judging the overall values, we attach greater significance to the BLYP absolute values because of their smaller error in the gas phase.

We have also considered some $AuAg_n$ clusters in these BLYP calculations on AgCl at the positive kink. These clusters generally have larger IP and EA values than just the pure Ag clusters. The Au_2 cluster has an EA 0.26 eV greater than Ag_2 and a much larger IP.

We have applied this BLYP method to several Ag_n, Au_n, and Ag_nAu clusters adsorbed to an Ag_4Br_4 embedded model of the AgBr positive kink. A pattern of energy levels similar to the results for AgCl is found. These are plotted in Figure 6. We observe an odd−even oscillation in the IP and EA of the Ag_n clusters. The calculated electron affinity is sufficiently large to accept an electron from the conduction band, but the Ag_2 and Ag_4 values give a trap depth of only a few tenths of an eV. Other patterns are very similar to AgCl. The Au_n clusters have much larger EA values than the Ag_n clusters and the same is true of AgAu. The corresponding ionization potentials are also larger, indicating an increase in stability.

We would like to emphasize the role of silver cluster relaxation, which is found when an electron is accepted from the conduction band. Our initial calculations treated the anion clusters as frozen at the geometry of the neutral adsorbed cluster. This is particularly crucial for Ag_2 since the electron affinity of this cluster is very close to the calculated crystal electron affinity. Without treating this relaxation the calculated EA of this cluster was often less than the calculated crystal EA. As an example for Ag_2 at the positive kink, the treatment of this relaxation increases the EA by 0.72 eV in Hartree−Fock and 0.32 eV in BLYP calculations on AgCl. For Ag the same calculations give increased EA values of 0.36 and 0.27 eV, respectively. The EA is increased by 0.50 eV by relaxation of Ag_2^- on the AgBr positive kink site. Treatment of this effect is important for properly describing the small Ag and Ag_2 adsorbed clusters. An idea of the amount of geometric relaxation can be obtained by comparing the final positions of neutral and anionic clusters given in Table 9. This effect is due to strong lattice coupling of the electron, as has been proposed by Hamilton.[39]

4. Discussion

We find a pattern of silver cluster electron affinity and ionization potentials that is in broad form, consistent with the nucleation and growth model of latent image formation. There are various sites on the cubic silver halide surfaces that impart distinct properties to the adsorbed silver cluster. The concept that kink sites have a partial charge and that double kink sites and flat terrace areas are roughly neutral in charge, is supported in these calculations. The values for the ionization potential and electron affinity of silver clusters are largest at the positive kink site, smaller at double kinks and flat sites and generally smallest at the negative kink site. This is found despite the fact that the optimized geometry and orientation of the silver cluster will vary from one site to another. It should be reiterated that in these calculations the lattice is allowed to polarize in response to the geometric surface site and possible charge on the silver cluster. The positive kink is unique among the different sites in providing electron accepting levels below the bottom of the calculated conduction band edge. These results support the long-held view[1] of special properties for these sites despite arguments that with only a half-charge in the high dielectic silver halide, the effects would be small. It is also useful to point out the consistency between the larger IP and EA values at the positive kink and the electrostatic driving force for collection of electrons at this site based upon the partial charge argument behind the steps in Figure 1.

We note that the pattern of IP and EA values calculated in Figures 5 and 6 are quite consistent for silver clusters at the positive kink between AgCl and AgBr. The larger IP value calculated for the adsorbed Ag atom may seem surprising because of its instability[36] in photographic experiments. Of course, the gas phase IP is 7.56 eV. This situation means that the Ag atom cannot easily transfer an electron to the conduction band. Rather, it must decay by loss of a silver ion followed by escape of the electron to the conduction band. Our estimates of the energy of this process shows that it depends upon the site of atom adsorption, but is about 0.6 eV at the positive kink. Thermal excitation at room temperature might be estimated to give a lifetime of about 1 ms for such a decay. Thus the Ag atom is not stable, but during its lifetime it may potentially capture an electron at the positive kink. The trap depth for such an electron is given by the value of the Ag atom EA relative to the crystal EA and is in the range 0.5−1.0 eV according to our calculations. Binding a silver ion to the intermediate Ag^-

species forms Ag_2 and greatly stabilizes this electron. According to the calculated IP values at the positive kink, this electron will be at or below the valence band edge. The Ag_2 can capture an electron from the conduction band with a depth of 0.5 eV or less. Thus, the Ag_2^- species so formed can reversibly release this electron because of its relatively shallow trap depth. Capture of a silver ion at this center will stabilize this electron in the Ag_3 cluster. Electron capture at Ag_3 is promoted by the relatively large EA value. We note that Ag_4 has a smaller EA than Ag_3, but larger than Ag_2, thus promoting growth at the larger clusters.

Clusters possessing IP values within the silver halide bandgap are susceptible to attack by photoholes present at the top of the valence band. This reaction is energetically allowed at Ag_3 and Ag_4 clusters on the positive kink and many of the clusters at other sites. Coulombic factors are expected to impede hole reactions at positive kink sites. Thus, removal of holes to prevent regression reactions, known in photography,[2b,41] would prevent this reaction. It is also known that infrared light exposure can bleach the latent image, which is thought to occur by exciting electrons from the cluster to the conduction band. The IP value of Ag_4 on the AgBr positive kink is about 2 eV from the conduction band edge, and that of Ag_3 is less. These values are consistent with threshold values quoted[41] for latent image bleaching, also known as the Herschel effect.

We have found that an important factor in electron capture by neutral silver clusters is their geometric relaxation. This deepens the electron trap depth by up to 0.5 eV. It is interesting to point out that Hamilton[1,39] had deduced the importance of this strong coupling of electrons to the silver halide lattice in earlier work. It was previously thought that electrons only weakly coupled to the silver halide lattice because self-trapping of the type observed for holes in AgCl in the bulk was not found for electrons. However, in the presence of the surface defect such as a kink or a small silver cluster, additional degrees of freedom are available for atom movement and apparently made use of when an electron is trapped.

Gold treatment of silver halide has long been known[41] to have effects on detecting the latent image. One study[42] to which attention is drawn was the experimental measurement of the critical size for development in a model system. Metal was evaporated onto an inert support, and using nucleation theory and microscope observations, the critical size for development was measured. This turned out to be Ag_4 and Au_2 for vacuum-deposited clusters and illustrates the role of gold. Our calculations for Au_2 and various AuAg clusters indicate the increase in IP and EA values brought about by the presence of gold versus pure silver clusters. An increased EA value of the small Au_2 cluster versus Ag_2 is consistent with electron acceptance from a reducing agent at a smaller critical size.

In earlier work[6] we have studied the energetics of latent image formation using semiempirical methods. These gave a qualitative picture of latent image formation similar to what has been derived here in more detail. A major shortcoming of the prior work was the lack of polarization correction for the crystal lattice. In the present work we accounted for this effect in our treatment of adsorbed clusters by the Hartree−Fock and density functional BLYP methods. Results from the latter two calculations are qualitatively similar, but have some numerical differences. Both methods agree on the special role of kink sites and trends in the IP and EA. Since the BLYP functional method gives much better agreement of calculated values for the gas phase, this method will be emphasized in future work.

There is no experimental measurement of the concentration of positive kinks on the cubic surface of AgCl or AgBr. Due to the negative surface charge[1] these sites are expected to be low in concentration. The equilibrium involving kinks and interstitial silver ion (Ag_i^+)

$$+K \leftrightarrow -K + Ag_i^+ \tag{9}$$

is thought to be rapid and so these kinks are expected to be constantly forming and decaying.

Our calculations have indicated a large electron affinity for adsorbed single silver atoms. At most sites, the single silver atom has a sufficient EA to capture a photoelectron from the conduction band. This result is consistent with a mechanism of concentrating electrons to start latent image growth to form the resulting Ag_2 center following addition of an interstitial silver ion. Of course, the single silver atom is unstable due to the driving force of silver ions escaping to other sites, as we indicated in reaction 2. It should also be noted that in this mechanism, agents that strongly bind silver ions would make single silver atoms less stable and this probably will decrease the number of latent image centers in any given grain. In this case, the second electron has a smaller probability of capture prior to decay of the silver atom. This decay mechanism for single silver atoms seems to be consistent with the interpretations of multiflash experiments of Kawasaki and Hada.[43] These workers found evidence that the silver atom lifetime is very sensitive to environmental reactions with O_2 and concluded that the activation energy for decay is not associated with the depth of the single-atom energy level. Furthermore, the deep IP level of the single silver atom is consistent with the conclusion from Monte Carlo types of simulation that the one electron state has the highest probability for existence as the atom.[44]

Larger neutral silver clusters are more stable than smaller silver clusters. This can be demonstrated in our data by including the calculated bond energy along with the relevant adsorption energies in Tables 2 and 3. For example, at the positive kink, Ag_2 is more stable than 2Ag by more than 1 eV in both AgCl and AgBr. Likewise, the Ag_3 and Ag_4 clusters are more stable than the separated atoms. This behavior is consistent with a model of nucleation and growth to larger silver clusters. The actual kinetics of these steps is very hard to determine, although the scheme in Figure 1 is a reasonable mechanism. These calculations indicate that neutral silver clusters at positive kink sites can capture photoelectrons and so there are no energy barriers due to thermodynamics in this mechanism. Following electron capture, an interstitial silver ion should rapidly neutralize the cluster. If silver ions were first adsorbed at the silver cluster, a very deep electron trap would result. Indeed, the EA of such a cationic cluster would be roughly equal to the IP of the neutral cluster. Under these circumstances, according to the calculated values in Figures 4 and 5, electrons could be trapped at cationic clusters on almost any of the different sites we have considered. This situation would promote multiple silver cluster formation upon photolysis, which would be a very inefficient form of photography. Thus, we argue that the neutral cluster adsorbed at the positive kink is the trapping center for photoelectrons.

We noted the photoionization experiments of Kawasaki et al.[10] that found oscillations in the IP of silver clusters on silver bromide grains. The threshold energies of 1.6, 0.75, and 1.1 eV were reported for Ag_2, Ag_3, and Ag_4, respectively. The atomistic calculations in Table 5 give 1.46, 0.92, and 1.91 eV for the same cluster sequence at the double kink. These values qualitatively agree with experiment and suggest double kinks as the possible adsorption sites for the clusters studied experimentally. They also rule out positive kink sites, where the calculated values are much larger, as being responsible for the

TABLE 11: Interatomic Potential Parameters Used for Atomistic Calculations

A. Interatomic Terms

interaction	A (eV)	ρ (A)	C (eV A^6)
$Ag^0 - Ag^+$	75999.6	0.229 7	348.9
$Ag^0 - Cl^-$	5012.9	0.341 21	464.6
$Ag^0 - Br^-$	5983.2	0.306 82	411.6

B. Silver−Silver Pair Potential in Various Clusters

cluster	A (eV)	ρ (A)	C (eV A^6)
Ag_2^+	19 073.48	0.321 19	2277.18
Ag_2^0	21 090.40	0.292 66	1366.47
Ag_2^-	17 824.38	0.308 34	1625.80
Ag_3^+	17 887.57	0.315 62	1919.61
Ag_3^0	17 720.64	0.290 86	1053.27
Ag_3^-	20 590.16	0.306 76	1872.12
Ag_4^+	14 520.33	0.316 18	1554.72
Ag_4^0	17 960.11	0.282 66	806.70
Ag_4^-	11 819.27	0.330 93	1757.20

TABLE 12: Adjustments (eV) Applied to IP/EA Data for Silver Halide Clusters on AgCl

A. Correction for Gas-Phase Calculation

	Hartree−Fock		BLYP	
cluster	ΔIP	ΔEA	ΔIP	ΔEA
Ag	1.32	1.70	−0.35	0.00
Ag_2	1.72	1.12	−0.28	−0.12
Ag_3	0.62	1.91	−0.66	0.16
Ag_4	2.01	0.93	−0.20	0.55

B. Lattice Polarization Terms

cluster	site	ΔIP	ΔEA
Ag	+K	−1.62	0.15
Ag_2		−1.86	0.32
Ag_3		−2.15	0.90
Ag_4		−2.19	1.22
Ag	−K	−0.55	1.91
Ag_2		−1.57	1.86
Ag_3		−1.96	1.82
Ag_4		−1.65	2.27
Ag	flat	−2.22	2.13
Ag_2		−1.95	1.87
Ag_3		−1.94	1.85
Ag_4		−1.92	1.82
Ag	−DK	−2.19	0.97
Ag_2		−1.61	1.28
Ag_3		−1.33	1.74
Ag_4		−1.11	0.84

experiments[10] threshold energies. On the whole, the agreement between calculation and experiment is reasonable when it is remembered that the particular sites studied in the experiments are not precisely defined.

Appendix

The interaction potentials have been computed by the Hartree−Fock method using correlation energy terms as described in the text. Table 11 contains the constants fitted to the Buckingham potential (eq 1). The procedure involved embedding an ion in a neutral hemispherical array of point charges positioned at silver halide lattice sites. A silver atom was positioned near the ion and the quantum mechanical procedure employed to determine energy as a function of distance. The potentials between gas-phase species were determined by using a uniform breathing motion to vary the internuclear distances. The linear structure for the trimer and square structure for the tetrameter in all charge states were examined. These structures are close in energy to the equilibrium gas-phase structure determined by calculation and were more convenient for fitting than the lower symmetry equilibrium structure. The total energy is divided by the number of pairwise interactions within a cluster to determine the pair potentials in Table 11.

TABLE 13: Mulliken Charges of Adsorbed Silver Clusters on Different Silver Chloride Surfaces Using Hartree−Fock Calculation

surface	quantum model	cluster size	cation	neutral	anion
+K	Ag_4Cl_4	1	+0.96	+0.03	−0.66
		2	+0.97	+0.04	−0.67
		3	+0.84	+0.02	−0.69
		4	+0.88	+0.01	−0.77
−DK	Ag_4Cl_5	1	+0.94	+0.01	−0.69
		2	+0.86	+0.01	−0.81
		3	+0.90	+0.01	−0.79
		4	+0.82	−0.07	−0.83
flat	Ag_5Cl_4	1	+0.85	+0.13	−0.77
		2	+0.70	+0.16	−0.90
		3	+1.03	−0.19	−0.97
		4	+0.99	−0.20	−1.03
−K	Ag_4Cl_4	1	+0.93	+0.02	−0.73
		2	+0.88	−0.01	−0.93
		3	+0.87	−0.05	−0.87
		4	+0.87	−0.06	−0.92

Table 12 contains the adjustment terms applied to each cluster size in order to calculate the IP and EA. The lattice polarization energies were determined by calculating the lattice relaxation energy for each charge state and taking the appropriate differences. The calculated adsorption energies for the various silver clusters of different charges were given in Tables 2 and 3. A complete energy minimization is used to achieve each configuration treated here. The adsorption energy corresponds to the change in energy from the relaxed adsorbed cluster to the separated relaxed surface and silver cluster. The calculated total bond energies for the relaxed clusters are

$$Ag_2^+ - 1.52 \text{ eV}, Ag_2^0 - 1.50 \text{ eV}$$

$$Ag_3^+ - 2.86 \text{ eV}, Ag_3^0 - 2.16 \text{ eV}$$

$$Ag_4^+ - 4.57 \text{ eV}, Ag_4^0 - 3.32 \text{ eV}$$

References and Notes

(1) (a) Hamilton, J. F. *Adv. Phys.* **1988**, *37*, 359. (b) Tani, T. *Photographic Sensitivity*; Oxford University Press: New York, 1995.

(2) (a) Bayer, B. E.; Hamilton, J. F. *J. Opt. Soc. Am.* **1965**, *55*, 439. (b) Hamilton, J. F. In *The Theory of the Photographic Process*, 4th ed.; James, T. H., Ed.; McMillan: New York, 1977. (c) Hamilton, J. F. *Photogr. Sci. Eng.* **1970**, *14*, 102. (d) Hailstone, R. K.; Liebert, N. B.; Levy, M.; Hamilton, J. F. *J. Imaging Sci. Technol.* **1988**, *32*, 150.

(3) (a) Hailstone, R. K. *J. Imaging Sci. Technol*. **1995**, *39*, 407. (b) Hailstone, R. K. *J. Phys. Chem*. **1995**, *99*, 4414. (c) Hailstone, R. K. *Comput. Phys.* **1994**, *8*, 205.

(4) (a) Moisar, E.; Granzer, F.; Palm, E. *J. Photogr. Sci.* **1977**, *25*, 12. (b) Malinowski, J. *Photogr. Sci. Eng*. **1979**, *23*, 99. (c) Moisar, E.; Granzer, F. *Photogr. Sci. Eng.* **1981**, *26*, 1. (d) Mitchell, J. W. *J. Imaging Sci. Technol*. **1995**, *39*, 193.

(5) (a) Brandt, R. C.; Brown, F. C. *Phys. Rev.* **1969**, *181*, 1214. (b) Eachus, R. S.; Olm, M. T.; Janes, R.; Symons, M. C. R. *Phys. Status Solidi* **1989**, *151*, 583. (c) Bennebroek, M. T.; Poluektov, O. G.; Zakrzewski, A. J.; Baranov, P. G.; Schmidt, J. *Phys. Rev. Lett*. **1995**, *74*, 442.

(6) (a) Baetzold, R. C. *J. Chem. Phys.* **1971**, *55*, 4363. (b) Baetzold, R. C. *Photogr. Sci. Eng.* **1975**, *19*, 11. (c) Hamilton, J. F.; Baetzold, R. C. *Photogr. Sci. Eng.* **1981**, *25*, 189.

(7) Flad, J.; Stoll, H.; Niklass A.; Preuss H. *Z. Phys. D* **1990**, *15*, 79.

(8) Dietz, F.; Koch, A.; Nieke, C.; Richter, R.; Reinhold: J.; Tadjer, A.; Tyutyulkov, N. *J. Imaging Sci.* **1986**, *30*, 146.

(9) Shelimov, K. B.; Safonov, A. A.; Bagaturyants, A. A. *Chem. Phys Lett.* **1993**, *201*, 84.

(10) Kawasaki, M.; Tsujimura Y.; Hada, H. *Phys. Rev. Lett.* **1986**, *57*, 2796.

(11) Alameddin, G.; Hunter, J.; Cameron, D.; Kappes, M. M. *Chem. Phys. Lett.* **1992**, *192*, 122.

(12) Taylor, K. J.; Pettiette-Hall, C. L.; Cheshnovsky, O.; Smalley, R. E. *J. Chem. Phys*. **1992**, *96*, 3319.
(13) (a) Tani, T.; Murofushi, M. *J. Imaging Sci.* **1994**, *38*, 1. (b) Guo, S.; Hailstone, R. K. *J. Imaging Sci.* **1996**, *40*, 210. (c) Tani, T. *Photogr. Sci. Eng.* **1972**, *16*, 35.
(14) (a) Balasubramanian, K.; Feng, P. Y. *Chem. Phys. Lett.* **1989**, *159*, 452. (b) Balasubramanian, K. *J. Mol. Struct.* **1989**, *202*, 291. (c) Liao, D.; Balasubramanian, K. *J. Chem. Phys*. **1992**, *97*, 2548.
(15) (a) Bonacic-Koutecky, V.; Fantucci, P.; Koutecky, J. *Chem. Rev*. **1991**, *91*, 1035. (b) Bonacic-Koutecky, L.; Cespiva, L.; Fantucci, P.; Koutecky, J. *J. Chem. Phys*. **1993**, *98*, 7981.
(16) Santamaria, R.; Kaplan, I. G.; Novaro, O. *Chem. Phys. Lett*. **1994**, *218*, 395.
(17) Bauschlicher, C. W.; Langhoff, S. R.; Partridge, H. *J. Chem. Phys*. **1990**, *93*, 8133; *J. Chem. Phys*. **1989**, *91*, 2412.
(18) (a) Norgett, M. J. Harwell Report AERE-R7015, 1972. (b) Catlow, C. R. A.; Mackrodt, W. C. *Computer Simulation of Solids*; Springer: Berlin, 1982. (c) Stoneham, A. M. *Theory of Defects in Solids:* Clarendon: Oxford, U.K., 1975.
(19) (a) Mott, N. F.; Littleton, M. J. *Trans. Faraday Soc.* **1938**, *34*, 481. (b) Lidiard, A. B. *J. Phys.: Condens. Matter* **1993**, *5*, 137.
(20) Tasker, P. W. *Philos. Mag.* **1979**, *39*, 119.
(21) Harding, J. H. *Rep. Prog. Phys*. **1990**, *53*, 1403.
(22) Baetzold, R. C.; Tan, Y. T.; Tasker, P. W. *Surf. Sci.* **1988**, *195*, 579.
(23) (a) Dick, B. G.; Overhauser, A. W. *Phys. Rev*. **1958**, *112*, 90. (b) Catlow, C. R. A.; Stoneham, A. M. *J. Phys. C* **1983**, *16*, 4321.
(24) (a) Jacobs, P. W. M.; Corish, J.; Catlow, R. A. *J. Phys. C: Solid State Phys*. **1980**, *13*, 1977. (b) Jacobs, P. W. M. *J. Imaging Sci.* **1990**, *34*, 79.
(25) Baetzold, R. C.; Catlow, C. R. A.; Corish, J.; Healy, F. M.; Jacobs, P. W. M.; Leslie, M.; Tan, Y. T. *J. Phys. Chem. Solids* **1989**, *50*, 791.
(26) Catlow, C. R. A.; Corish, J.; Harding, J. H.; Jacobs, P. W. M. *Philos. Mag. A* **1987**, *55*, 481.
(27) Seitz, F. *Rev. Mod. Phys.* **1951**, *23*, 328.
(28) Baetzold, R. C. *Phys. Rev. B* **1995**, *52*, 11424.
(29) (a) Becke, A. D. *Phys. Rev*. **1988**, *A33*, 3098. (b) Lee, C.; Yang, W.; Parr, R. G. *Phys. Rev. B* **1988**, *37*, 785. (c) Johnson, B. G.; Gill, P. M.; Pople, J. A. *J. Chem. Phys.* **1993**, *98*, 5612.
(30) Sakai, Y.; Miyoshi, E.; Klobukwski, M.; Huzinaga, S. *J. Comput. Chem*. **1987**, *8*, 256.
(31) Baetzold, R. C.; Eachus, R. S. *J. Phys.: Condens. Matter* **1995**, *7*, 3991.
(32) CADPAC: The Cambridge Analytical Derivatives Package Issue 6, Cambridge, 1995. A suite of quantum chemistry programs developed by Amos, R. D. with contributions from I. L. Alberts, J. S. Andrews, S. M. Colwell, N. C. Handy, D. Jayatilaka, P. J. Hnowles, R. Kobayashi, K. E. Laidig, G. Lasming, A. M. Lee, P. E. Maslen, C. W. Murray, J. E. Rice, E. D. Simandiras, A. J. Stone, M. D. Seu, and D. J. Tozer.
(33) Hansen, J.; Marchetti, A. P.; Mason, M. G. Private communication.
(34) Bauer, R. S.; Spicer, W. E. *Phys. Rev. Lett*. **1970**, *25*, 1283.; *Phys. Rev. B* **1976**, *14*, 4539.
(35) (a) Moser, F.; Urbach, F. *Phys. Rev*. **1956**, *102*, 1519. (b) Marchetti, A. P.; Burberry, M. S. *Phys. Rev. B* **1988**, *37*, 10862.
(36) Webb, J. H. *J. Opt. Soc. Am*. **1933**, *23*, 157.
(37) Ran, J.; Schmude, R. W.; Gingerich, K. A.; Wilhite, D. W.; Kingcade, J. E. *J. Phys. Chem*. **1993**, *97*, 8535.
(38) Deri, R. J.; Spoonhower, J. P.; Hamilton, J. F. *J. Appl. Phys.* **1985**, *57*, 1966.
(39) Hamilton, J. F. *J. Imaging Sci*. **1990**, *34*, 1.
(40) Gibb, R. M.; Rees, G. J.; Thomas, B. W.; Wilson, B. L. H.; Hamilton, B.; Wright, D. R.; Mott, N. F. *Philos. Mag.* **1977**, *36*, 1021.
(41) Kellogg, L. M. In *The Theory of the Photographic Process*, 4th ed.; James, T. H., Ed.; McMillan: New York, 1977.
(42) Hamilton, J. F.; Logel P. C. *Photogr. Sci. Eng.* **1974**, *18*, 507.
(43) Kawasaki, M.; Hada, H. *J. Imaging Sci.* **1985**, *29*, 132.
(44) Hamilton, J. F. *Photogr. Sci. Eng.* **1983**, *27*, 225.